Real-Time Data Acquisition and Signal Processing of a Multistatic mm-Wave Radar System

Jochen Moll [#], Marion Böswirth [*], Viktor Krozer [#], Jürgen Bosse [*]

[#]Goethe University of Frankfurt, Department of Physics, Terahertz Photonics Group, Max-von-Laue-Strasse 1, 60438 Frankfurt am Main (Germany), Phone: +49 (0) 69 798-47208, E-Mail: moll@physik.uni-frankfurt.de
[*]Robo-Technology GmbH, Benzstrasse 12, 82178 Puchheim, Germany

***Abstract*—In this paper, we report on the challenging real-time data acquisition and signal processing of a multistatic 100 GHz millimeter-wave radar system with 32 Tx- and 32 Rx-elements. With four ACQ216CPCI Digitizer Boards it is possible to sample 32 channels simultaneously with 14-bit resolution at a maximum sampling rate of 25 MSPS. Moreover, data pre-processing in form of a matched filter is performed on hardware level in real-time to reduce the amount of data that must be transferred to the PC which executes the backprojection algorithm for 3D-imaging.**

***Index Terms*—MIMO radar, Microwave imaging, Data acquisition, Signal processing**

I. Introduction

The mmRadar4Space-project, funded by the German Aerospace Center (DLR), aims at a three-dimensional imaging radar for space applications that can be used to image and track a non-cooperative object, e.g. a satellite. By means of the imaging sensor shown in Fig. 1 docking maneuvers can be performed independently of the lighting situation. Therefore, a sparse array consisting of 32 transmitters and 32 receivers are used to actively illuminate the unknown scene at an operating frequency of 100 GHz. The 32 transmitters are placed on two horizontal lines where each line consists of 16 transmitting antennas with equidistant spacing. In order to synthesize a higher number of receiver elements and to facilitate higher image quality, the 16 receivers on the left and right side of the panel can be linearly manipulated through a linear motorized stage.

In the literature, several multistatic millimeter wave radars can be found. Most of them are designed for remote sensing purposes either in security or non-destructive testing applications. A full electronic active real time imager at 72 to 80 GHz is presented in [1] to detect concealed objects. The modularized setup consists of multiple clusters and each cluster contains 46 Tx and 46 Rx antennas. Another system uses an optimized multistatic array for short range applications [2]. Here, the frequency range is between 75 and 90 GHz. A 300 GHz millimeter wave radar system with 8 Tx and 16 Rx antennas for stand-off distances of around 7 m is documented in [3]. Moreover, an active scanning system for stand-off distances of 4 m and 25 m working at 662-688 GHz is proposed in [4]. Synthetic focusing improves the depth resolution in non-destructive testing applications [5]. Here, three-dimensional reconstructions with the global back-projection algorithm are presented for a homogeneous styrodur sample with distributed defects, operating in the frequency range between 230 GHz and 320 GHz. A flexible millimeter-wave radar system at 94 GHz is documented in [6], where the image quality of different antenna arrangements has been compared. The Golay-9 configuration revealed the best reconstruction quality compared to star, circular and cross-shaped constellations.

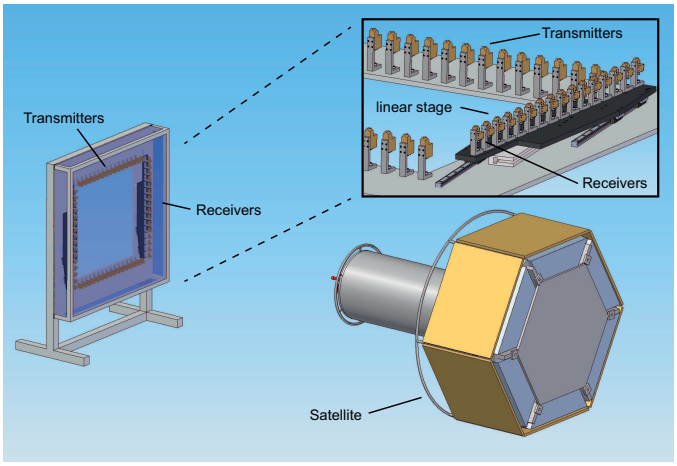

Fig. 1. 3D-CAD view on the imaging sensor and a non-cooperative satellite; Zoomed part shows the mechanical shift unit to linearly manipulate the receiver positions to obtain a higher number of receiver positions, after [7].

The contribution of this paper is to present the real time data acquisition and signal processing architecture of the setup in Fig. 1. Therefore, Section II introduces the utilized waveforms followed by a discussion of the data acquisition hardware in Section III. Finally, experimental calculations on the dedicated hardware will be shown in Section IV in conjunction with imaging results in noisy environments.

II. Waveform Design

A property of time divisision multiplexing is given by the fact that only one antenna transmits at the same time. The receiver signal is less complex because no contributions from other sources occur. A challenge for code division multiplexing systems with widely spaced antennas, such as the one presented here, is that all Tx elements send a unique code sequence simultaneously. Hence, the receiver signal is a

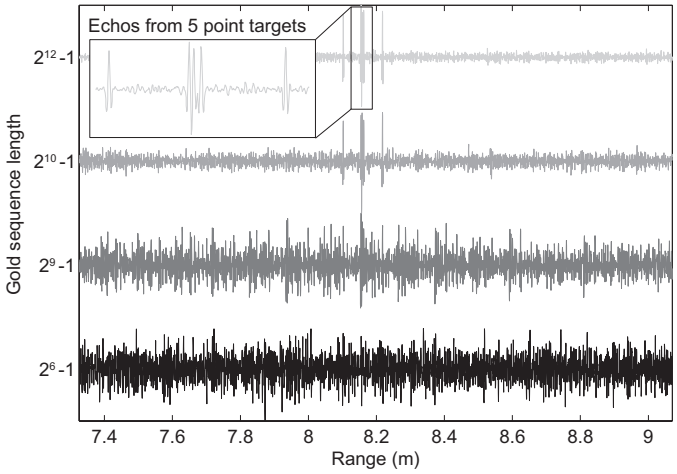

Fig. 2. The strong measurement noise masks the echoes in the matched filter responses when the Gold codes are short. Increasing the code length provides a clear identification of the echoes while the noise amplitude remains constant.

mixture of time-shifted and attenuated signals from all transmitting antennas. Crucially for the code design are excellent correlation properties with minimum sidelobes. A lot of work especially in the MIMO communication society has been conducted to find codes with optimum correlation properties [8]. In this work, we apply Gold sequences because they have excellent cross-correlation properties. Moreover, a large set of sequences can be generated while the corresponding code length is short.

Our MIMO-radar is based on a code-multiplex approach where all transmitting antennas send in parallel a unique pseudo-noise sequence. The phase-modulated bipolar Tx-codes are known at the receiver so that a matched filter [9] can be applied. Fig. 2 illustrates an application of Gold sequences in a noisy environment. Strong measurement noise masks the echoes in the matched filter responses when the Gold codes are short. Increasing the code length provides a clear identification of the echoes while the noise amplitude in this example remains constant. On the other side, longer codes cause a longer measurement time and higher signal processing costs. Hence, a trade-off must be found for real-time operation between SNR and processing time.

III. Data Acquisition Architecture

Fig. 3 shows the preliminary experimental setup that consists of a signal generator, four ACQ216CPCI Digitizer Boards from D-TACQ and a PC. The input data for the signal generator, i.e. the Gold-code mentioned in the previous section, is an export file created by mathematica. The signal generator reads the signal data from file and creates the phase-modulated Gold sequence at the desired carrier frequency. With the four ACQ216CPCI Digitizer Boards from D-TACQ [10] shown in Fig. 4 it is possible to sample 32 channels simultaneously with 14-bit resolution at a maximum sampling rate of 25 MSPS. Each board contains an Intel XScale Microprocessor, 1GByte Ram and a Xilinx Virtex II Pro FPGA for transferring ADC-

Fig. 3. Preliminary experimental setup.

Fig. 4. Four ACQ216CPCI Digitizer Boards from D-TACQ enable parallel data acquisition for 32 receiver channels.

data to memory and to implement DSP co-processing features.

A simplified digital subsystem of a single ACQ216CPCI unit is shown in Fig. 5. The ADC Array samples the incoming down-converted signals simultaneously with eight channels without multiplexing. The record length is defined by 128k-samples at a sampling rate of 20MSPS. The primary function of the FPGA is the data transfer of ADC data to the DDRAM. In order to accelerate the process of calculation, the data processing is distributed among the XScale microprocessor and the FPGA. After applying the DSP algorithms, the tremendous amount of data is reduced significantly and can be handed over to the PC via Ethernet. This data are the real-values range profiles, compare Fig. 3, that are used subsequently for the image formation process.

The main effort of calculation refers to the Fast Fourier Transform (FFT) which must be known for all channels to determine the matched filter responses. The required number of additions and multiplications mostly depend on the number of transmitters N_T, receivers N_R and the number of samples per channel N. Therefore, the Radix-2-FFT algorithm is used, which needs $N/2 \cdot log(N)$ multiplications and $N \cdot log(N)$ additions. The minimum effort to calculate the cross correlation function for the full configuration of 32 Tx and 32 Rx is 11.3 GOPS (giga operations per second) for the additions and 3.9 GOPS for the multiplications. Exploiting the real-valued nature of the range profiles by using symmetry properties of the DFT, a further reduction of the computational time for the FFT can be achieved.

IV. Results

A. Comparing Matched Filter Implementations

The first step was a floating point implementation of the cross-correlation function on the destination hardware. This implementation is very time-consuming and unsuitable for the final operation, but it shows that the hardware samples the data properly. Comparison of noisy data recorded from a preliminary experimental setup shown in Fig. 3 between the floating point and mathematica calculation is shown in Fig. 6(a). This example is based on 2 transmitters, 1 receiver and a binary phase-modulated Gold-sequence with a code

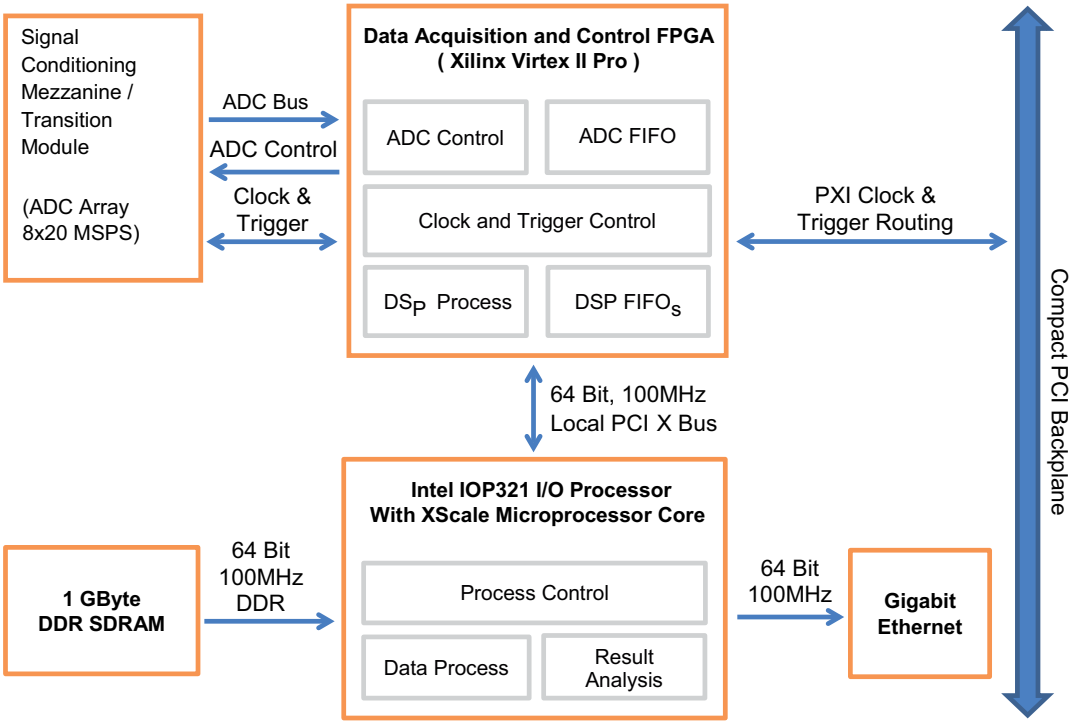

Fig. 5. Four ACQ216CPCI Digitizer Boards from D-TACQ enable parallel data acquisition for 32 receiver channels.

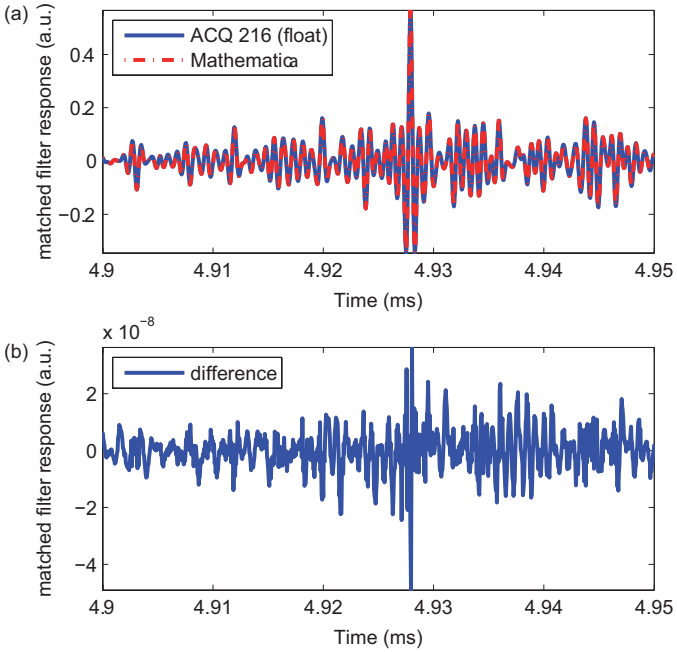

Fig. 6. (a) Matched filter response of an experimental signal calculated on ACQ216CPCI-hardware with a floating point calculation and mathematica (b) Difference signal.

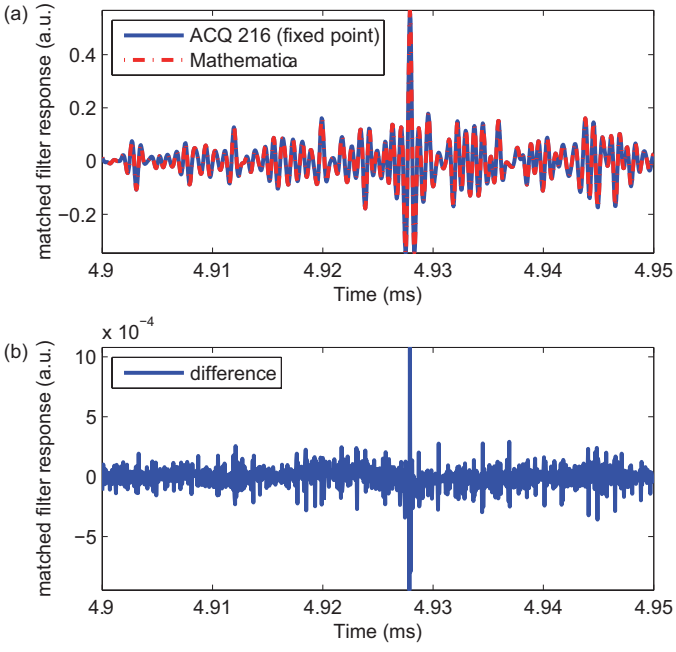

Fig. 7. (a) Matched filter response of an experimental signal calculated on ACQ216CPCI-hardware with a fixed-point calculation and mathematica (b) Difference signal.

length of $2^6 - 1$. It can be concluded that almost identical results can be achieved. Small deviations can be observed in the differential signals shown in Fig. 6(b) where the maximum difference is $3.62 \cdot 10^{-08}$, i.e. a relative error of $6.4 \cdot 10^{-06}$ %.

The time consuming FFT algorithm was improved by implementing a fixed-point calculation in C-language and assembler code. This resulted in enormous time-savings at the expense of calculation precision. The delay for the floating-point FFT of 38.4 s could be reduced to 1.2 s and 0.4 s, respectively.

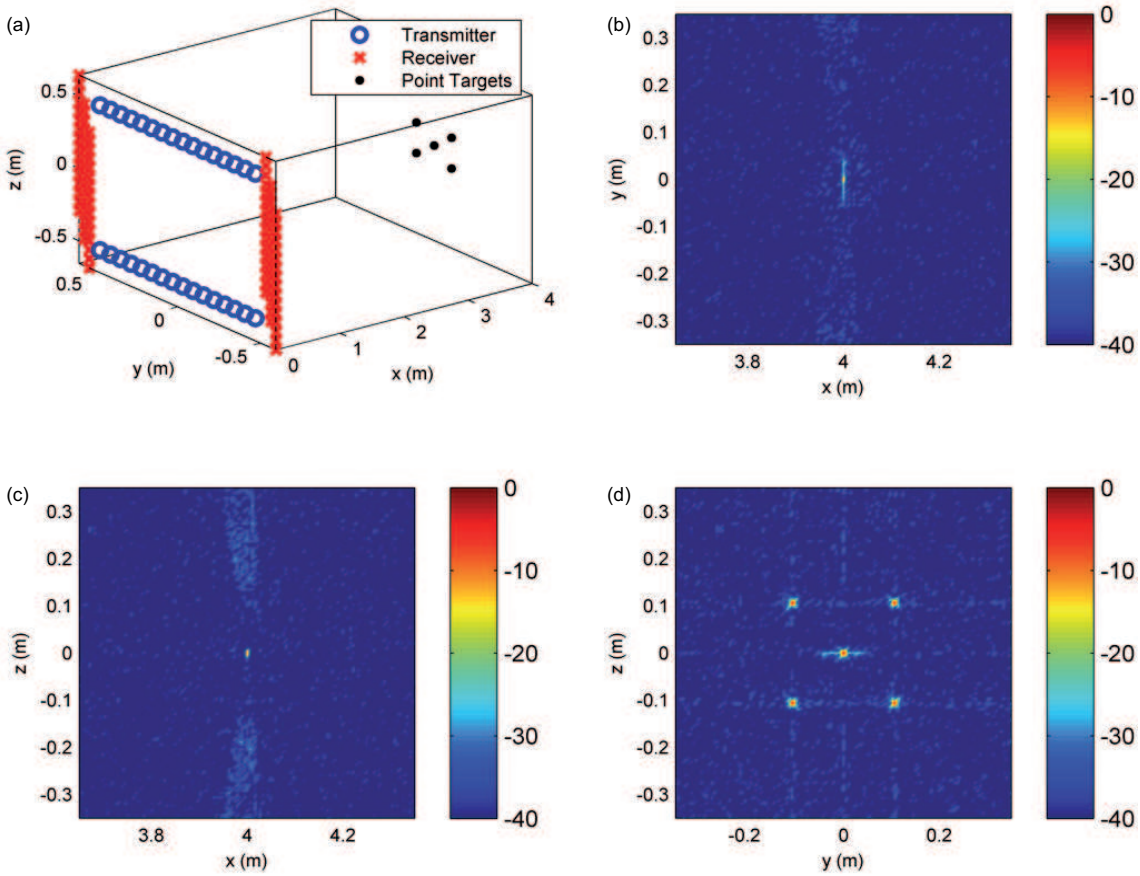

Fig. 8. Three dimensional imaging example for a code length of 2^6-1 and the same strong measurement noise as shown in Fig. 2: (a) Antenna configuration and point target location, (b)-(d) planar cross-sections through the three-dimensional reconstruction volume at the position of the center point target. All five point targets can be identified correctly via coherently summing over all Tx-Rx-elements.

A range-profile comparison of the same signal is shown in Fig. 7(a). The fixed-point implementation is compared against the mathematica results. A maximum and acceptable deviation of $1.08 \cdot 10^{-03}$, i.e. a relative error of 0.19 %, is shown by the differential signal in Fig. 7(b).

B. Imaging in Noisy Environments

Fig. 8 demonstrates the performance of the imaging radar with simulated measurements and strong superimposed measurement noise. In this example 32 transmitters send binary phase-modulated Gold sequences with a code length of 2^6-1 elements. A total number of 96 synthesized receivers positions have been employed as shown in Fig. 8(a). In order to evaluate the imaging performance, three planar cross-sections through the three-dimensional reconstruction volume have been determined. It can be concluded from Fig. 8(b)-(d) that all five point targets can be clearly detected with a dynamic range of 40 dB. Fig. 9 illustrates a zoom-in of Fig. 8(c) in order to show the accurate imaging result of a point target.

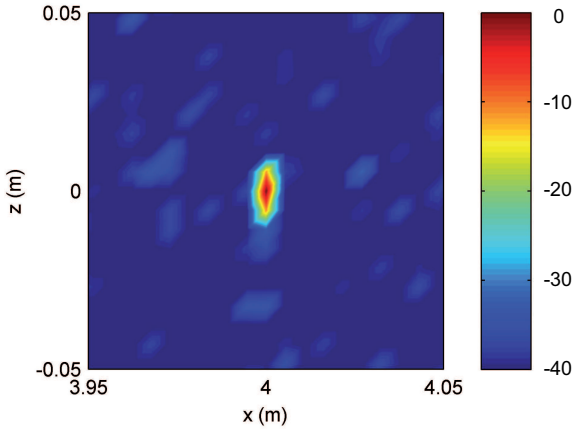

Fig. 9. Zoom-in of the image reconstruction from Fig. 8(c).

V. Conclusions and Outlook

This paper presented the data acquisition and signal processing infrastructure of a multistatic 100 GHz imaging radar system with 32 Tx and 32 Rx elements. A trade-off for real-time operation is shown between the length of the employed pseudo-noise sequence and signal-to-noise ratio. Finally, three-dimensional imaging results in a noisy environment were presented where five point targets can be clearly identified.

ACKNOWLEDGEMENT

The authors wish to acknowledge the financial support of the mmRadar4Space-project that is funded by the German Aerospace Center (DLR). Viktor Krozer is grateful for funding by Oerlikon AG.

REFERENCES

[1] S. Ahmed, A. Schiessl, and L.-P. Schmidt, "A novel fully electronic active real-time imager based on a planar multistatic sparse array," *IEEE Transactions on Microwave Theory and Techniques*, vol. 59, no. 12, pp. 3567–3576, 2011.

[2] F. Gumbmann and L.-P. Schmidt, "Millimeter-wave imaging with optimized sparse periodic array for short-range applications," *IEEE Transactions on Geoscience and Remote Sensing*, vol. 49, no. 11, pp. 3629–3638, 2011.

[3] J. Moll, P. Schöps, and V. Krozer, "Towards three-dimensional millimeter-wave radar with the bistatic fast-factorized back-projection algorithm - potential and limitations," *IEEE Transactions on Terahertz Science and Technology*, vol. 2, no. 4, pp. 432–440, 2012.

[4] K. Cooper, R. Dengler, N. Llombart, T. Bryllert, G. Chattopadhyay, E. Schlecht, J. Gill, L. C., A. Skalare, I. Mehdi, and P. Siegel, "Penetrating 3-d imaging at 4- and 25-m range using a submillimeter-wave radar," *IEEE Transactions on Microwave Theory and Techniques*, vol. 56, no. 12, pp. 2771–2778, 2008.

[5] A. Keil, T. Hoyer, J. Peuser, H. Quast, and T. Loeffler, "All-electronic 3d thz synthetic reconstruction imaging system," in *36th International Conference on Infrared, Millimeter, and Terahertz Waves*, 2011.

[6] W. Caba and G. Boreman, "Active Sparse-Aperture Millimeter-Wave Imaging Using Digital Correlators," *Journal of Infrared, Millimeter and Terahertz Waves*, vol. 32, pp. 434–450, 2011.

[7] J. Moll, M. Kotiranta, B. Hils, and V. Krozer, "A 100 ghz millimeter wave radar system with 32 transmitters and 32 receivers for space applications," in *42nd European Microwave Conference (EuMC)*, Amsterdam, The Netherlands, 2012 (accepted, May 2012).

[8] A. Mitra, "On pseudo-random and orthogonal binary spreading sequences," *International Journal of Information Techniques*, vol. 4, no. 2, pp. 137–144, 2008.

[9] L. S.F., J. Chen, L. Zhang, and Y. Zhou, "Application of complete complementary sequence in orthogonal mimo sar system," *Progress In Electromagnetics Research C*, vol. 13, pp. 51–66, 2010.

[10] D-TACQ Solutions, http://www.d-tacq.com/acq216cpci.shtml.